Gas Processing Journal

Vol. 9, No. 2 2021, pp. 113 -130
http://gpj.ui.ac.ir

Research Paper

Exergoeconomic and Exergoenvironmental Evaluation of a Turbo-Compressor Station using Solar Energy and Exhaust Gas Heat Recovery

Mohammad Hassan Khoshgoftar Manesh [1,2], Hamed Cheragh[2], S. M. A. Mousavi Tabar[2], Marc A Rosen[3]

[1] Division of Thermal Science & Energy Systems, Department of Mechanical Engineering, Faculty of Technology & Engineering, University of Qom, Qom, Iran

[2] Center of Environmental Research, University of Qom, Qom, Iran

[3] Faculty of Engineering and Applied Science, University of Ontario Institute of Technology, Oshawa, Ontario, L1G 0C5, Canada

Received: 2021-10-07 Revised: 2022-08-23 Accepted: 2022-09-13

Abstract: Compressor stations are needed to transport gas through a pipeline, which consumes a significant amount of energy. To improve the efficiency of the compressor stations, the heat recovery of gas exhaust has been applied using the heat recovery of the steam generator (HRSG). Three types of HRSG as a single, dual, and triple-pressure combined cycle with a reheat system have been investigated. In this regard, the fuel heating and also preheating of feed water using solar energy have been evaluated. Due to the application of solar power tower technology to achieve 1000ºC temperature for hybridization in conventional fossil-fired power, it has been considered. Also, exergoeconomic and exergoenvironmental analyses of using solar energy and heat recovery of the gas exhaust have been evaluated. The arrangement of the gas station is based on (3+1) gas turbines. In this regard, an HRSG system and a steam turbine were used for three gas turbines in the Kashan pipeline station to recover of hot gas in the outlet of the gas turbine.

keywords: Solar Energy, Gas turbine, Heat Recovery, Pipeline Gas Station, Turbo-compressor, Exergoenvironmental analysis.

1. Introduction

In order to transport gas, several compressor stations and kilometers of pipelines are needed. These compressor stations typically consume a high amount of energy. The main component in a compressor station is a gas turbine that drives the turbo-compressor. The high-temperature exhaust gases from the gas turbines can be recovered to improve the efficiency of the compressor station.

Numerous studies have been performed on the recovery of gas turbines exhaust gases and using solar energy as follows. Khoshgoftar Manesh et al. [1] evaluated different desalination systems such as multi-effect desalination. In that work, they developed and evaluated various scenarios considering economic, exergetic, and exergoeconomic viewpoints. Shahzad et al. [2] demonstrated the use of thermocline energy in a MED system. They suggested this green desalination technology be used in tropical areas. Askari and Ameri [3] investigated the integration of a Rankine cycle with a solar field and a MED system. The Rankine cycle was used to generate electricity, the solar field was utilized to provide a part of the thermal energy needed in the Rankine cycle. The MED system was included in this hybrid system to produce fresh water. In that work, they presented an economic analysis for their hybrid system and determined the amount of fuel saving. Elsayed et al. [4] modeled different configurations of the MED system in steady and dynamic operation. They also added a thermal vapor compressor and studied other configurations. Comparing to the other arrangements, parallel cross feed showed a better

* **Corresponding Author. M. H. Khoshgoftar Manesh**
Authors' Email Address: M. H. Khoshgoftar Manesh (m.khoshgoftar@qom.ac.ir)، **H. Cheragh (**hd.cheragh72@gmail.com**), S. M. A. Mousavi Tabar (**sr.mousavitabar@chmail.ir**), M. A. Rosen (**marc.rosen@ontariotechu.ca**)**

2345-4172/ © 2022 The Authors. Published by University of Isfahan
This is an open access article under the CC BY-NC-ND/4.0/ License (https://creativecommons.org/licenses/by-nc-nd/4.0/).

http://10.22108/GPJ.2022.130903.1109

functioning regarding ratio of output gain and specific heat consumption.

Lianying et al. [5] offered a mathematical model for a cogeneration system in order to produce power and water at the same time. They developed an algorithm in order to solve their model. They optimized their system economically and minimized the total annual cost. A numerical work on a desalination system was presented by Shahzad et al. [6]. In their study, they combined a multi-effect desalination cycle with an adsorption desalination cycle and so they presented a MEDAD cycle. They compared this MEDAD cycle with different types of MEDs and observed an increase in the production rate of this hybrid cycle. Sadri et al. [7] suggested a mathematical model for a MED system with thermal vapor compression and an RO (MED+TVC+RO). They presented an exergy analysis for the RO system and investigated its performance for seawater. In their study, the performance of the RO membrane was predicted by using a computational model. They also investigated the exergy destruction and exergetic efficiency of their hybrid system and selected the optimum design of the MED-RO system. Askari et al. [8] discussed a Linear Fresnel (LF) solar field as multi-effect desalination cycle with a thermal vapor compression system from the point of view of technoeconomic feasibility. They reported that when they increased the solar energy consumption the cost of water production increased. They also reported a 180% reduction in the levelized cost of water when there was a 12-fold increase in multi-affected desalination thermal vapor compression (MED-TVC). A MED-based desalination process, entitled DBMED was developed by Dastgerdi et al. [9]. They reported that their system produces up to 45% more freshwater compared to an optimized conventional MED. In comparison with the flash-boosted multi-effected desalination (FBMED), the system decreased the normalized pumping power consumption (*NPPC)* by 38%. An exergy-based analysis of a hybrid system was presented by Mokhtari et al. [10]. They designed a system for covering the electricity and water demand o a rural area. For this purpose, they used a gas turbine cycle, a multi-effect desalination cycle, and a reverse osmosis system.

Kostowski et al. [11] proposed some strategies in order to enhance the thermodynamic performance of a natural gas compressor station. They suggested using the waste heat of a compressor station for covering the hot water demand of a plant. Their second suggestion was to use this waste heat to run an Organic Rankine Cycle (ORC). They demonstrated that the ORC unit saves a significant amount of energy. Although it is not economically feasible to have the ORC unit under partial operating condition. Bianchi et al. [12] investigated the integration of an Organic Rankine Cycle (ORC) and a compressor station. They presented a technoeconomic analysis and their study showed that the payback period of the ORC cycle is in 7 years. They concluded that using an ORC unit in their system is profitable and on the other hand it can recover a significant amount of waste heat. Gomez Alaez et al. [13] investigated the integration of an ORC unit with a compressor station. In their study, they discussed the methodology of computing the energetic performance of the system.

Yanvarev et al. [14] proposed a solution to improve compressor station performance. They targeted the compression stage and suggested using a cooling process. In their analysis, they showed that it is possible to lower the energy utilization with fan drives by 20-30%. Akbari et al. [15] proposed and analyzed a cogeneration system. They found that this system can produce power and refrigeration at the same time as a cogeneration cycle or only be a refrigeration system. Hanafi et al. [16] studied a combined cogeneration power plant. In their work, they developed an EES code to study the thermal performance of this cycle. They developed an economic model for capital cost and operation and maintenance cost, and it was proven that the cycle they presented could save about 20.6% of the total annual cost.

An investigation of modifying a gas turbine cogeneration plant was done by Dabwan et al. [17]. in that work they focused on a solar system and they simulated a solar power cycle using thermoflow software. They also presented a thermoeconomic analysis for their hybrid system and showed that an integrated solar natural gas power plant can reduce the electricity cost by 76-85%. Their study also revealed that integration of linear Fresnel reflector solar field with the power plant can reduce CO_2 annual emission by 18%. A study of several energy sources such as nuclear and fossil power plants was presented by Rezaei et al. [18]. In their study, six different energy source plants were chosen to present an economic evaluation for coupling a desalination system with them. They proved that the electricity of the combined cycle plant costs 30% more than PWR and PBMR.

In this study, recovery of gas turbine exhaust has been investigated by using HRSG and steam turbine to provide power. Furthermore, solar tower technology has been applied to preheat water. Energetic, exergetic, exergoeconoic and exergoenvironmental modeling and analyses are performed on a turbo-compressor station using solar energy and exhaust gas heat recovery.

2. System Description

A MAPNA MGT-30MD (25 MW) Turbo

Compressor was chosen to model the main gas-turbine power generation cycle. Turbo compressor units use a natural gas-fired turbine to turn a centrifugal compressor. We used Engineer Equation Solver (EES) and the assumptions proposed by Bejan et al. [19] to model the gas-turbine power generation cycle. The specification of the turbo-compressor station in Kashan is determined in Table 1. Also, Figure 1 shows the turbo-compressor cycle.

Table 1 Input data of MGT-30MD turbo compressor

Parameter	Value
ISO rated power	25.7 MW
Efficiency	35.20%
Heat rate	10227 kJ/kWh
Turbine inlet temperature	1241 °C
Exhaust gas temperature	487 °C
Exhaust gas mass flow	89 kg/s
Pressure ratio	21.44
Power turbine speed	5000 rpm
Power turbine stages	2
Turbine dimensions	6.3 m × 2.3 m × 2.3 m

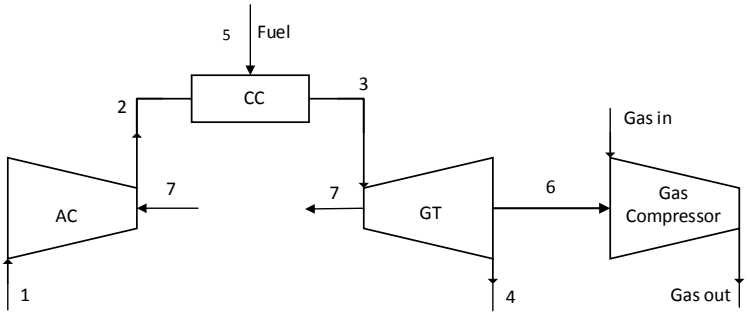

Figure 1 Schematic diagram of the turbo compressor

2.1. Solar Section

Due to using solar heating through solar tower technology, we used the following equations in order to determine the amount of required solar energy for the Brayton cycle.

$$\eta_{coll} = \frac{\dot{Q}_{useful}}{DNI(t_s) \times n \times A_{mirror}} \quad (1)$$

$$\eta_{coll} = \eta_{Reciver} \times \eta_{Field} \quad (2)$$

$$\eta_{Field} = \eta_{cos} \times \eta_{atten} \times \eta_{shadow} \times \eta_{block} \times \eta_{refl} \quad (3)$$

$$\eta_{Reciver} = \eta_{spill} \times \eta_{absorp} \times \eta_{rad} \times \eta_{conv} \times \eta_{cond} \quad (4)$$

According to equation (1), to calculate the input heat from the solar field, we need to calculate the parameters and the efficiencies of the receivers and solar field. Note in equation (1) that n is the number of mirrors and A_{mirror} is the area of each mirror. Equation (3) shows the field efficiency where η_{cos} shows the efficiency based on cosine, η_{shadow} indicates shadowing, η_{block} expresses blocking, η_{refl} shows reflectance and η_{atten} is atmospheric attenuation. The different modes of loss in the receiver are shown in Figure 6. Equation (4) shows the receiver efficiency where η_{spill} indicates the spillage of the receiver, η_{absorp} shows the amount of absorption, η_{rad} expresses radiation, η_{conv} shows convection and η_{cond} denoted conduction losses. As shown in Figure 2, cosine efficiency is the most important factor in an optimum field layout. This factor is dependent on the positions of the sun and heliostats.

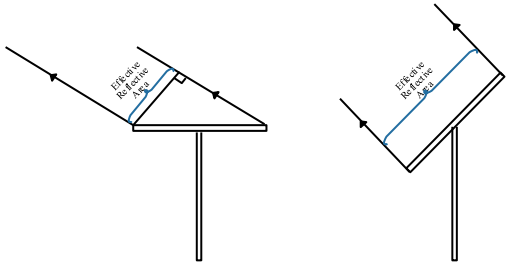

Figure 2 Efficient area of heliostat at different times [20]

A heliostat that is behind another is affected by the shadowing factor which occurs at low sun angles. According to Figure 3, blocking occurs when the light beam is blocked by a mirror that is in front of another mirror. These two factors are functions of the sun angle, heliostat spacing, and the distance of the receiver of the tower from the ground.

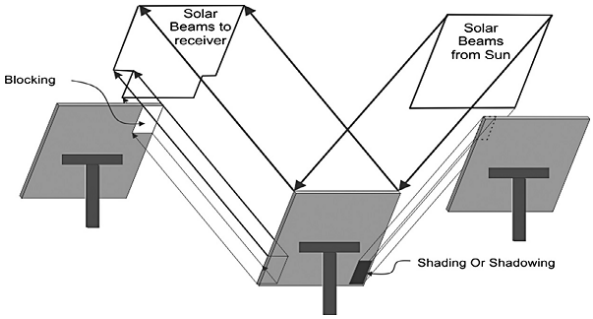

Figure 3 Effect of shadowing and blocking on a heliostat [20]

The atmospheric transmittance loss (η_{atten}) occurs due to the attenuation of the beam that is reflected from a heliostat as it goes to the tower. The other important loss factor is atmospheric attenuation. In a large heliostat field where the receiver is far from the heliostats the atmospheric attenuation loss is remarkable. The distance at which atmospheric attenuation occurs is shown in Figure 4.

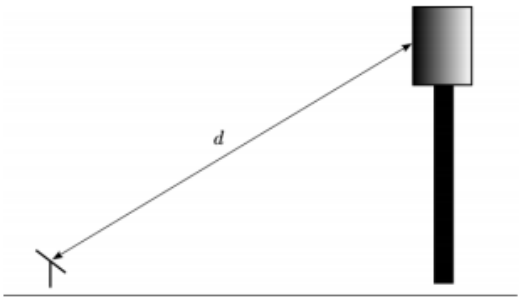

Figure 4 Distance at which atmospheric attenuation occurs for a heliostat relative to the solar tower

The energy directed to the solar tower that does not reach the absorbing area depends on the heliostat field (heliostat beam focus and distance from the tower) and the receiver (size of absorbing surface or aperture). Increasing the receiver size can result in a reduction in terms of spillage loss. Although the size of the receiver is limited by convection and radiation losses which are proportional to the area of the receiver. These two losses are functions of the operating temperature of the system and the receiver size. Therefore they affect the design of the receiver. Absorption loss is practically between 0.95 and 0.98. Radiation and convection are the biggest concern for a receiver in terms of energy loss. Hottel's clear-day model which is described in Appendix A was used in this study. The Hottel model may be extended to other climate types. The assumptions proposed by Soltani et al. [20] for the Kashan site came in

Table 2.

Figure 5 shows the best arrangement for heliostats which is a radial pattern. Minimizing the usage of the land, blocking, and shadowing are the benefits of this pattern. Mechanical interference happens when heliostats are packed tightly around the tower. In order to prevent this from happening the heliostats must be separated from each other sufficiently. The spacing must be increased for heliostats that are located at a longer distance from the tower.

Due to the increase in calculations by adding the solar section, we have to use the regression equation (5). Figure 6 shows the amount of net heat absorbed by a receiver, considering the losses.

Table 2 Assumptions for Kashan Location

Location of field	Kashan, Gas Compressor Station, Iran	Long	80
		Lat	33.59
		Alt	987
		GTM	5
Heliostat area	4×4 m^2		
Receiver cluster area	120 m^2		
Tower height	150		
η_{refl}	0.9		
$\eta_{receiver}$	0.56		
$\eta_{shadowing}$	1		
$\eta_{blocking}$	1		
η_{cos}	Depends on the number of mirrors		
η_{atten}	Depends on the number of mirrors		

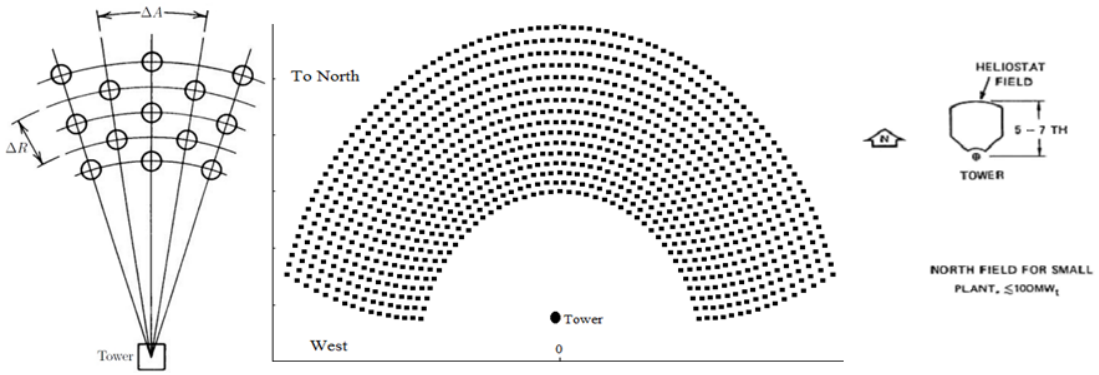

Figure 5 Radial pattern for heliostats [20]

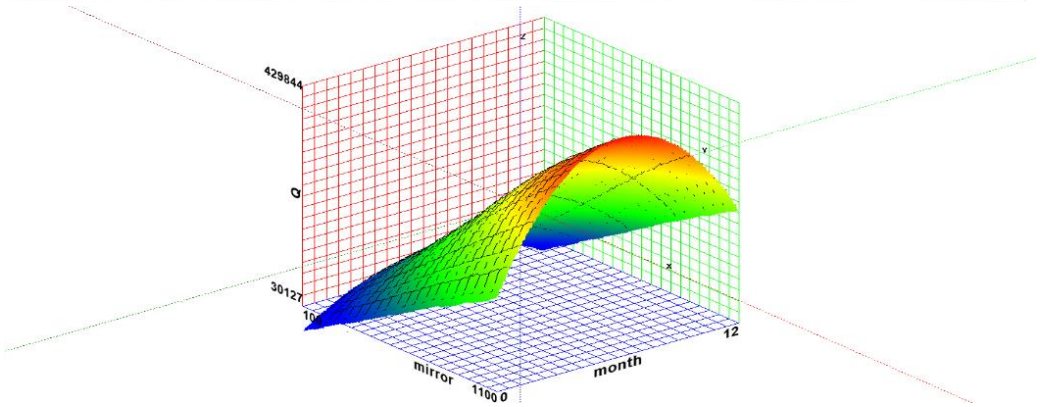

Figure 6 Heat generated in a receiver of the solar tower

$$Q = -1.099 \times 10^5 + 3.628 \times 10^2 \times n - 6.533 \times 10^{-3} \times n^2 + 4.736 \times 10^4 \times m - 3.642 \times 10^3 \times m^2 - 3.276 \times n \times m \left(\frac{w}{m^2}\right) \quad (5)$$

3. Thermodynamic Modeling

In this section, thermodynamic models for three different pressure levels of combined cycles with a reheat system have been discussed [21, 22].

3.1. Single-pressure combined cycle with reheat system

Single-pressure reheat consists of ESO, EVA, and SH. In the first section (ECO), the inlet water is pumped to the desired pressure. It will be heated to reach the saturated liquid state. We have a water-steam mixture in the EVA section which is separated by a drum. It exists in form of saturated liquid and saturated steam. Note that water circulation in EVA is through a pump other than the main pressure pump. Saturated steam at the exit of EVA goes into the superheating section. This steam is used to drive the steam turbine. Figure 7 depicts a combined cycle with a reheat system with different pressure levels. The equations used for the single pressure system came in Table 3.

General assumptions for single-pressure reheat are as follows:

- Ambient-air pressure is 1.013 bar, and the temperature is 25°C.
- Steam is condensed at a pressure corresponding to a temperature that is 10°C over the environmental temperature.
- The mixture of water and steam that enters the EVA drums ultimately turns into saturated water and saturated vapor.
- The steam output quality of the steam turbine is considered to be 0.88.
- The isentropic efficiencies for the steam turbines and hydraulic pumps are set at 0.90 and 0.85 respectively.
- The temperature differences of pinch-point (PP_1) are fixed at 10 K.
- The dew point temperature of the exhaust gases is considered to be 65°C.
- The isentropic efficiency equations can be used for the pump and turbine.

3.2. Dual-pressure combined cycle with reheat system

A dual-pressure reheat combined-cycle generates steam at two levels of pressure. It consists of two ECO heat exchangers, two drums, two EVAs, two SH exchangers, and an RH exchanger. The flue gas enters the heat recovery steam generator at point 4g, and the heat transferred in this process produces steam at point 9s. The produced steam at point 9s enters the high-pressure turbine at point 10s. Steam expands at the outlet of the steam generator and it goes into the HP steam turbine at a temperature of 11s. in this stage the reheat steam reaches a higher temperature of 12s. the steam expands at 12s in the LP steam turbine, then it goes into the condenser. After the condenser, we have saturated water at 1s which is pumped and reaches a higher pressure. The water absorbs heat at 2s and goes into the steam drum. The drums separate saturated steam from saturated water. The saturated water then returns to the generator and the saturated steam is superheated at 5s. This superheated steam expands in the LP steam turbine and reaches the pressure of the condenser at 6s. The saturated water passes through drum 1 and drum 2, then enters the economizer at 8s and absorbs heat. This saturated water which is heated then evaporates in the generator. The saturated steam in drums is superheated then and reaches a higher temperature at 10s [21, 22].

The diagram in Figure 8 demonstrates five pinch-points where the changes in temperature for heat transfer being predicted to have a minimum value. Applying the energy balance equation for 5 Sections of the steam generator provides the following equations. Equations used for the dual pressure system are presented in Table 4.

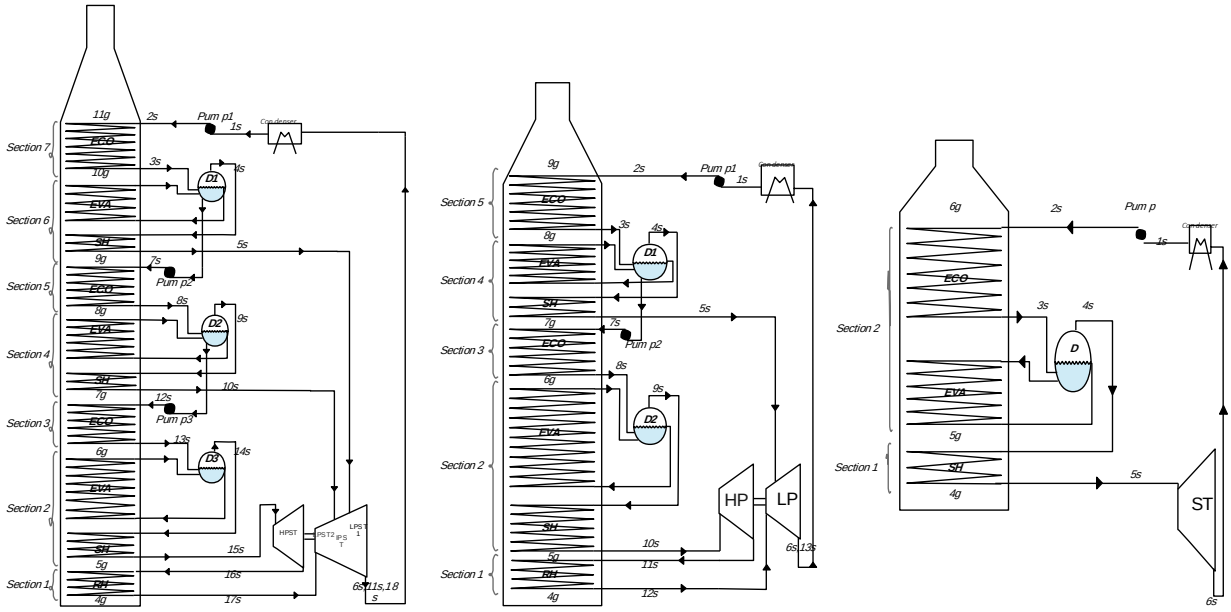

Figure 7 Single, dual and triple-pressure combined cycle with reheat system

Table 3 Equations used for single-pressure combined-cycle with reheat system

Energy conservation equations for sections 1 and 2		Temperature difference	
$\dot{m}_g(h_{g5} - h_{g6}) = \dot{m}_s(h_{s3} - h_{s2})$	(6)	$PP_1 = T_{g5} - T_{s3}$	(8)
$\dot{m}_g(h_{g4} - h_{g5}) = \dot{m}_s(h_{s5} - h_{s3})$	(7)	$PP_2 = T_{g6} - T_{s2}$	(9)

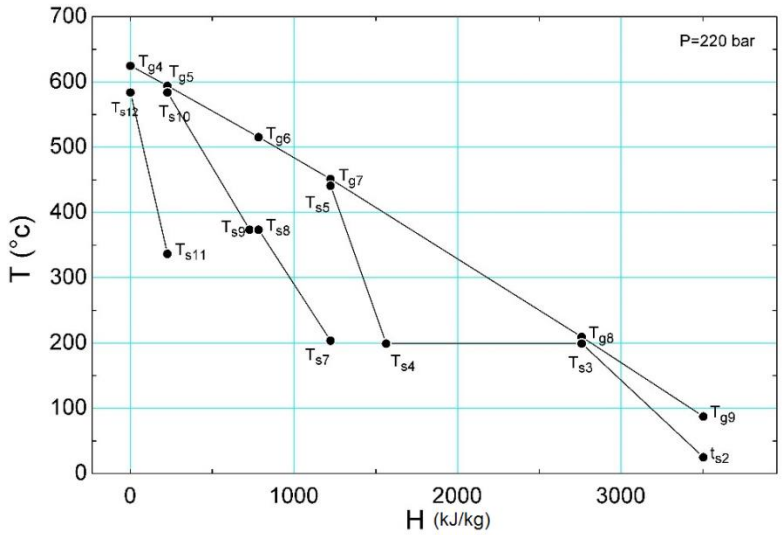

Figure 8 T-H diagram for the dual-pressure combined cycle with reheat system

Table 4 Equations used for dual-pressure combined-cycle with reheat system

Energy conservation equations for sections 1 – 5		Temperature difference	
$\dot{m}_g(h_{g4}-h_{g5})=(\dot{m}_s-\dot{m}_{sD1})(h_{s12}-h_{s11})$	(10)	$PP_1=T_{g5}-T_{s10}$	(15)
$\dot{m}_g(h_{g5}-h_{g6})=(\dot{m}_s-\dot{m}_{sD1})(h_{s10}-h_{s8})$	(11)	$PP_2=T_{g6}-T_{s8}$	(16)
$\dot{m}_g(h_{g6}-h_{g7})=(\dot{m}_s-\dot{m}_{sD1})(h_{s8}-h_{s7})$	(12)	$PP_3=T_{g7}-T_{s5}$	(17)
$\dot{m}_g(h_{g7}-h_{g8})=\dot{m}_{sD1}(h_{s5}-h_{s3})$	(13)	$PP_4=T_{g8}-T_{s3}$	(18)
$\dot{m}_g(h_{g8}-h_{g9})=\dot{m}_s(h_{s3}-h_{s2})$	(14)	$PP_5 = T_{g9} - T_{s2}$	(19)

The design assumptions are as flows:

- The following equation shows the temperature of evaporation for drum 1. In this equation, T_{sD2} is the evaporation temperature of drum 2 and T_c is condensing temperature.

$$T_{sD1} = \frac{T_{sD2} + T_c}{2} \quad (20)$$

- The input pressure of the drum is set at 220 bar.
- A minimum temperature difference of 10 K is set for pinch point 1. To reduce the irreversibility, the minimum values were considered for PP_3 and PP_4, which are 10 K and 20 K respectively.
- The pressure ratio of reheating (a) was set at 0.2.

3.3. Triple-pressure combined cycle with reheat system

As demonstrated in Figure 9 the diagram for the triple-pressure combined-cycle with reheat system is the same as the dual-pressure. In this section, we only discuss thermodynamic relations and assumptions. The reheat combined cycle has 3 heat exchangers of economizer type, 3 evaporators, 3 superheaters, and a preheater [22]. The equations used for the dual pressure system are presented in Table **5**.

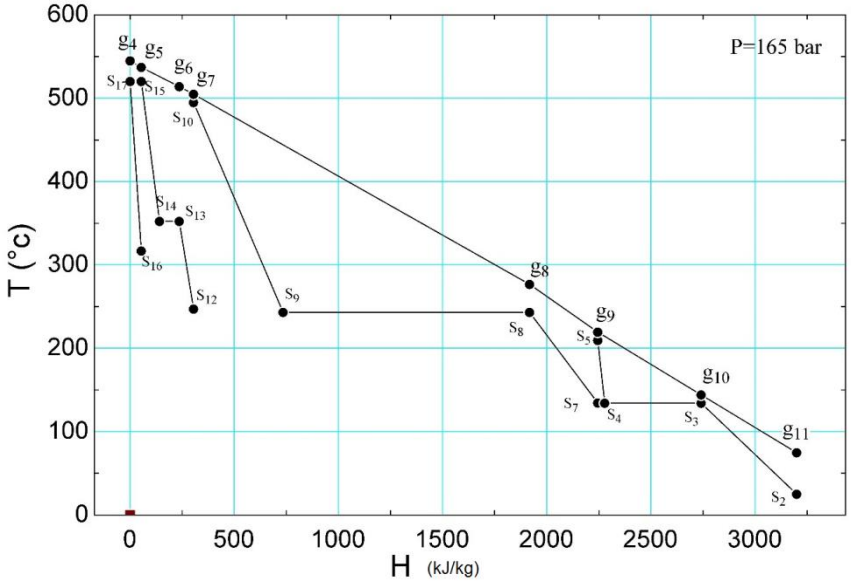

Figure 9 T-H diagram for the triple-pressure combined cycle with reheat system

Table 5 Equations used for dual-pressure combined-cycle with reheat system

Energy conservation equations for sections 1 - 7		Temperature difference	
$\dot{m}_g(h_{g4}-h_{g5})=(\dot{m}_s-\dot{m}_{sD1}-\dot{m}_{sD2})(h_{s17}-h_{s16})$	(21)	$PP_1=T_{g5}-T_{s15}$	(28)
$\dot{m}_g(h_{g5}-h_{g6})=(\dot{m}_s-\dot{m}_{sD1}-\dot{m}_{sD2})(h_{s15}-h_{s13})$	(22)	$PP_2=T_{g6}-T_{s13}$	(29)
$\dot{m}_g(h_{g6}-h_{g7})=(\dot{m}_s-\dot{m}_{sD1}-\dot{m}_{sD2})(h_{s13}-h_{s12})$	(23)	$PP_3=T_{g7}-T_{s10}$	(30)
$\dot{m}_g(h_{g7}-h_{g8})=\dot{m}_{sD2}(h_{s10}-h_{s8})$	(24)	$PP_4=T_{g8}-T_{s8}$	(31)
$\dot{m}_g(h_{g8}-h_{g9})=(\dot{m}_s-\dot{m}_{sD1})(h_{s8}-h_{s7})$	(25)	$PP_5=T_{g9}-T_{s5}$	(32)
$\dot{m}_g(h_{g9}-h_{g10})=(\dot{m}_{sD1})(h_{s5}-h_{s3})$	(26)	$PP_6=T_{g10}-T_{s3}$	(33)
$\dot{m}_g(h_{g10}-h_{g11})=(\dot{m}_s)(h_{s3}-h_{s2})$	(27)	$PP_7=T_{g11}-T_{s2}$	(34)

Design assumptions are as follows:

- The temperature differences for pinch-point 3 (PP_3) are set at 10 K. To reduce the irreversibility, PP_5 and PP_6 were set at their minimum values.
- The pressure of the third drum is considered to be 165 bar.
- The pressure ratio of reheating (a) is set at 0.2.
- We can set the PP_1 temperature difference at its minimum value which is 10 K or we can consider the minimum temperature difference of

the superheater which is 25 K..

$$\delta T_{superheat} = T_{g4} - T_{s17} = 25 \quad (35)$$

- The highest value is set for the reheat steam temperature which is 584°C.
- The evaporation temperatures of drum 1 and drum 2, are set at the average temperature of the condensing temperature and the evaporation temperature of drum D_3. The temperatures of evaporation for drum 1 and drum 2 are fixed so that

$$T_{seD_1} = T_c + \Delta T \quad (36)$$

$$T_{seD_2} = T_c + 2\Delta T \quad (37)$$

Here,

$$\Delta T = \frac{T_{sD3} - T_c}{3} \quad (38)$$

where T_c is the temperature of condensing and T_{sD3} is the temperature of evaporation for drum D_3.

4. Analysis

4.1. Thermodynamic analysis

The thermodynamic analysis is the first step in the study of energy systems. Mass and energy balance are provided for each piece of equipment and the control volume of the total system. Using thermodynamic analysis for each component, thermodynamic properties such as enthalpy, entropy, temperature, and pressure of each flow can be calculated. Enthalpy and entropy are thermodynamic properties that depend on temperature and flow pressure.

4.2. Exergy analysis of the system

Exergy is the maximum theoretical energy that is available to be used. As a result, it is considered to be the basis for cost allocation of the system flows [19]. The thermodynamic analysis of the system based on the second law is called the exergy analysis. The main parameters of exergy of the system are physical exergy, chemical exergy, potential exergy, and kinetic energy [19, 23]. The total exergy of the system is as follows:

$$E = E^{PH} + E^{CH} + E^{PT} + E^{KN} \quad (39)$$

The specific exergy is defined as the ratio of exergy to mass and can be written as:

$$e = e^{PH} + e^{CH} + e^{PT} + e^{KN} \quad (40)$$

In this paper, kinetic and potential exergies are neglected. So, the equation is generally written as follows:

$$e = (h - h_0) - T_0(s - s_0) + e^{CH} \quad (41)$$

In most systems, the control volume is monitored in a steady state. Therefore, the expression ofthe exergy balance in a stable state is important.

$$0 = \sum_j \dot{E}_{q,j} - \dot{W}_{cv} + \sum_i \dot{E}_i - \sum_e \dot{E}_e - \dot{E}_D \quad (42)$$

The first two terms in the equation above are considered to be zero due to the assumption of adiabatic components.

4.3. Exergetic variables

In order to evaluate and optimize a thermal system, we need to determine the exergy difference and a sufficient method for determining the cost for each component of the system. The following equation shows the exergetic efficiency that is expressed as the ratio of product to fuel.

$$\varepsilon_k = \frac{\dot{E}_{P,k}}{\dot{E}_{F,k}} \quad (43)$$

The exergy destruction based on the fuel product concept and the rate of exergy destruction is demonstrated in the equations below.

$$\dot{E}_D = \dot{E}_F - \dot{E}_P - \dot{E}_L \quad (44)$$

$$y_{D,k} = \frac{\dot{E}_{D,k}}{\dot{E}_{F,total}} \quad (45)$$

4.4. Thermoeconomic analysis

In thermoeconomic analysis, exergy is the basis for allocating costs. The cost rate for each flow is obtained from the multiplication of the exergy rate of the stream. A cost balance is often presented for the system in economic analysis.

$$\sum \dot{C}_{product,k} = \sum \dot{C}_{Fuel,k} + \dot{Z}_k \quad (46)$$

The exiting exergy cost rate is equal to the cost rate of entering exergy and the operating and maintenance cost $\dot{Z}^{OM}_K$ and capital investment $\dot{Z}^{CI}_K$ [19].

$$\dot{Z}_K = \dot{Z}^{CI}_K + \dot{Z}^{OM}_K \quad (47)$$

In each section, if we consider the number of unknown outputs as (N) then we need (N-1) supplementary equations [24].

4.5. Economic modeling

In the economic analysis of a system, the annual cost of investment, fuel costs, and maintenance costs for the system should be considered. In the present section, the total revenue requirement (TRR) of the system was applied for the economic analysis of the system. The total revenue requirement (TRR) comes to the sum of the following amounts: fuel costs and operating and maintenance expenses, total capital recovery, insurance, preferred stock, taxes, and the minimum rate of return for common equity investment [19].

$$TRR_L = CRF \sum_{i=1}^{BL} \frac{TRR_j}{(1+i_{eff})^i} \quad (48)$$

$$TRR_j = TCR_j + ROI_j + FC_{j,elec} + FC_{j,steam} + OMC_j + ITX_j + OTXI_j \quad (49)$$

In the equation above, TRR_j is the requirement of total income in each year of the economic system's life. The capital recovery factor is defined as follows [19].

$$CRF = \frac{i_{eff}(+i_{eff})^{BL}}{(1+i_{eff})^{BL}-1} \quad (50)$$

The levelized fuel cost is determined from the multiplication of fuel cost in the first year that the system operates, in a constant value. The levelized operating and maintenance costs are determined from the multiplication of fuel, operating, and maintenance in the first year that system operates, in a constant value [19]. The levelized carrying charges are expressed as:

$$CC_L = TRR_L - FC_L - OMC_L \quad (51)$$

Finally, to calculate ($\dot{Z}_k$), the following equation proposed by Colpan [25] was used.

$$\dot{Z}_k = \frac{OMC_L + CC_L}{\tau} \cdot \frac{PEC_K}{\sum PEC_K} \quad (52)$$

$$\tau = CF \times 365 \times SH \quad (53)$$

Since we have a hybrid system, the operating time of the solar section is during the day. To express the operating time, a specific value should be considered, which is the average amount of time in a year and equals 9.67 hours for a day, though it is considered to be 24 for the other components. The corresponding equations for Purchased Equipment Cost (PEC) are shown in Appendix B. The assumptions used in economic analysis are shown in Table 6.

Table 6 Assumptions used in economic analysis. [26]

Constant	Value
Interest rate	5%
CF	0.85
lifetime	30 years
Inflation rate	5%

4.6. Exergoenvironmental analysis

Exergoenvironmental analysis is a method that combines the exergy concept and evaluation of a system's life cycle. This analysis reveals the location, magnitude, and causes of thermodynamic inefficiencies in a cycle. The component-related environmental impact ($\dot{Y}_k$), is related to the components used in the system. The Eco-indicator 99 is utilized to calculate the component-related environmental impact in the current study. It must be noted that the assessment of environmental impacts will always be treated differently and are often unreliable. An exergoenvironmental analysis is usually performed in the same way as an exergoeconomic analysis [27]. The component-related environmental impact $\dot{Y}_k$ takes into consideration the whole lifespan of the component and comprises the contributions below which are shown in Appendix C.

$$\dot{Y}_k = \dot{Y}_k^{CO} + \dot{Y}_k^{OM} + \dot{Y}_k^{DI} \quad (54)$$

$$\dot{B}_{product,k} = \dot{B}_{Fuel,k} + \dot{Y}_k \quad (55)$$

In the equation above, $\dot{Y}_k^{CO}$ is the environmental impact which includes the construction, $\dot{Y}_k$ comprises the operation and maintenance, and $\dot{Y}_k^{DI}$ includes the environmental impact. The environmental impact rate that is in association with the exergy is demonstrated as follows:

$$\dot{B}_k = b_k \cdot \dot{E}_k \quad (56)$$

The environmental impact rate associated with the exergy destruction can be expressed as follows:

$$\dot{B}_D = b_{Fuel,K} \cdot \dot{E}_{D,K} \quad (57)$$

$$r_{b,k} = \frac{b_{p,k} - b_{F,k}}{b_{F,k}} = \frac{1-\varepsilon_k}{\varepsilon_k} + \frac{\dot{Y}_k}{\dot{B}_{F,k} - \dot{B}_{D,k}} \quad (58)$$

$$\varepsilon_k = \frac{\dot{E}_{P,k}}{\dot{E}_{F,k}} = 1 - \frac{\dot{E}_{D,k}}{\dot{E}_{F,k}} \quad (59)$$

$$y_{D,k} = \frac{\dot{E}_{D,k}}{\dot{E}_{F,total}} \quad (60)$$

6. Computer Computation

The computer code has been developed in EES software as shown in the flow diagram in Figure 10. In this figure, thermodynamic modeling of the turbo compressor and the system combined with it is evaluated first. Then the calculations related to the solar sector are done in order to integrate the two systems. Then, the relevant information is used to determine the geographical location so that the data needed to determine the weather conditions of the desired location are determined. Then the modeling of the integrated system is done in three pressure modes based on the first law of thermodynamics. After this part's calculations, the integrated system's analysis and evaluation are done for the second law of thermodynamics. After determining the quality of energy, economic and environmental calculations are done considering the appropriate assumptions for the system based on the results of exergy analysis.

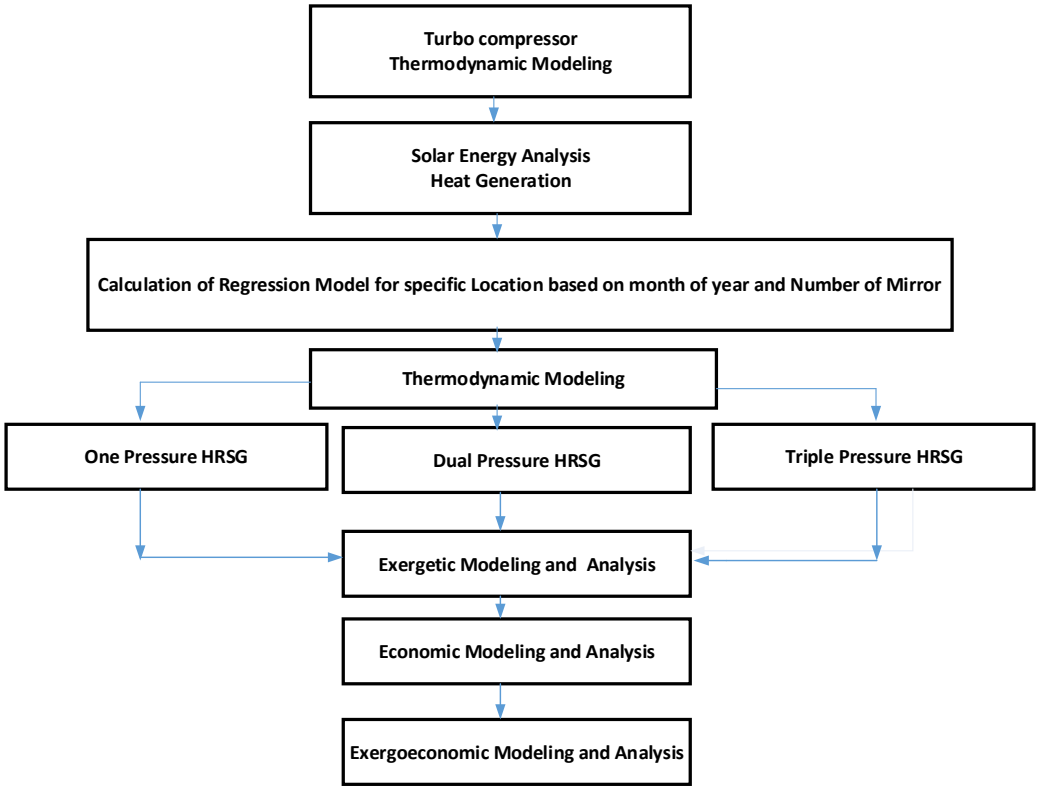

Figure 10 Flow diagram of how the problem is solved step by step

Device	$\dot{E}_{F,k}$ (MW)	$\dot{E}_{P,k}$ (MW)	$\dot{E}_{D}$ (MW)	ε_k (%)	$y_{D,k}$ (%)	$\dot{C}_{D,k}$ ($/h)	$\dot{Z}_k$ ($/h)	f_k (%)	r_k (%)	$\dot{B}_{D,k}$ (mPts/h)	$\dot{Y}_k$ (mPts/h)	$f_{b,k}$ (%)	$r_{b,k}$ (%)
AC	43.91	41.84	2.076	95	4.73	140.5	1212	89.6	47.7	45676	360.9	0.78	75
CC	117.9	90.39	27.52	77	23.34	1303	5.62	0.42	30.5	405172	964.7	0.23	71.21
GT	72.92	68.91	4.004	95	5.5	306.9	157.1	33.8	8.7				
Solar	3.89	2.084	1.78	54	45.16	498.8	972	66	253	186373	57890	23	112
HRSG	17.72	14.97	2.75	84	15.53	267.6	152.8	34.5	28.2	54598	127.9	0.23	18.42
Cond ST	14.24	12.89	1.38	90	9.7	183.9	226.4	53.3	23	34313	866.5	2.5	11

7. Results

Thermodynamic verification of the present study has been performed comparing the results of Ref [20] and [30]. Results show that high accuracy has been achieved with both of them. Tabel 7 shows the data of exergy destruction ($\dot{E}_D$), exergetic efficiency (ε_k), exergy destruction ratio ($y_{D,k}$), cost rate of exergy destruction ($\dot{C}_{D,k}$), total cost rate of component (sum of cost rates associated with capital investment operating and maintenance expenses) ($\dot{Z}_k$), exergoeconomic factor ($\dot{Z}_k$), relative cost difference (r_k), environmental impact rate that is in association with the exergy destruction ($\dot{B}_{D,k}$), component-related environmental impact ($\dot{Y}_k$), exergoenvironmental factor ($f_{b,k}$) and the exergoenvironmental relative parameter ($r_{b,k}$) of single-pressure reheat arrangement without solar energy. Similar parameters were shown for dual-pressure and triple-pressure in Table 8 and Table 9 respectively. The data of the system while using 500 mirrors for single, dual, and triple-pressure are given in, Table 11, and Table 12 respectively. Table 13, Table 14, and Table 15 show the data of single, dual, and triple-pressure while using 1000 mirrors in the solar field.

The combustion chamber (CC) has the highest amount exergy destruction ($\dot{E}_D$) in all cases. Consequently, this leads to the highest cost rate of exergy destruction ($\dot{C}_{D,k}$) in this component. The lowest cost rate of exergy destruction for dual and triple-pressure cycles is at the back-pressure steam turbine, whereas in single-pressure cycles the lowest amount is at the air compressor. According to Table 7, the lowest amount for exergy destruction for the single-pressure cycle without solar energy is at the air compressor, whereas in dual-pressure and triple-pressure without using mirrors and while using 500 and 1000 mirrors this parameter is minimum at back pressure steam turbine as shown in Tables 8-15. The lowest amount ofexergy

destruction in single-pressure cycles while using 500 and 1000 mirrors is at condensing steam turbine as illustrated in Reference source not found and Table 13.

The higher total cost rates ($\dot{Z}_k$) are at the air compressor and solar section and the lowest amount is at the combustion chamber in all cases. The highest component-related environmental impact ($\dot{Y}_k$) in systems without a solar field is at condensing steam turbine (Cond ST) whereas in cycles with the solar field this parameter is the highest at the solar section. HRSG has the lowest amount of component-related environmental impact in all cases except for the dual-pressure cycles in which the lowest amount is at the air compressor.

Table 7 Single-pressure reheat arrangement without solar energy

Device	$\dot{E}_{F,k}$ (MW)	$\dot{E}_{P,k}$ (MW)	$\dot{E}_D$ (MW)	ε_k (%)	$y_{D,k}$ (%)	$\dot{C}_{D,k}$ ($/h)	$\dot{Z}_k$ ($/h)	f_k (%)	r_k (%)	$\dot{B}_{D,k}$ (mPts/h)	$\dot{Y}_k$ (mPts/h)	$f_{b,k}$ (%)	$r_{b,k}$ (%)
AC	43.91	41.84	2.076	95	4.73	143	1254	89.7	48.5	45676	360.9	0.78	75
CC	117.9	90.39	27.52	77	23.34	1325	5.814	0.44	30.6	405172	964.7	0.23	71.21
GT	72.92	68.91	4.004	95	5.5	312	162.5	34.2	8.83				
HRSG	14.83	12.53	2.302	84	15.53	267.6	138.3	34.1	27.9	54598	127.9	0.23	18.42
Cond ST	35.73	32.25	3.465	90	9.7	549	307	35	24	102939	1384	1.3	11

Table 8 Dual-pressure reheat arrangement without solar energy

Device	$\dot{E}_{F,k}$ (MW)	$\dot{E}_{P,k}$ (MW)	$\dot{E}_D$ (MW)	ε_k (%)	$y_{D,k}$ (%)	$\dot{C}_{D,k}$ ($/h)	$\dot{Z}_k$ ($/h)	f_k (%)	r_k (%)	$\dot{B}_{D,k}$ (mPts/h)	$\dot{Y}_k$ (mPts/h)	$f_{b,k}$ (%)	$r_{b,k}$ (%)
AC	43.91	41.84	2.076	95	4.73	130	1038	88.8	44.5	45676	360.9	0.78	5
CC	117.9	90.39	27.52	77	23.3	1212	4.813	0.4	30.6	405172	964.7	0.23	71.2
GT	72.92	68.91	4.004	95	5.5	285	134.5	32	8.5				
HRSG	15.92	14.06	1.854	88	11.7	188	219	54	28	43976	570.1	1.3	13.4
BP ST	5.442	5.124	0.32	39	5.9	45	140.3	75	64.6	9090	1291	12	8.7
Cond ST	34.83	31.44	3.378	39	9.7	474	388.3	45	32.4	96090	1980	2	11.2

Table 9 Triple-pressure reheat arrangement without solar energy

Device	$\dot{E}_{F,k}$ (MW)	$\dot{E}_{P,k}$ (MW)	$\dot{E}_D$ (MW)	ε_k (%)	$y_{D,k}$ (%)	$\dot{C}_{D,k}$ ($/h)	$\dot{Z}_k$ ($/h)	f_k (%)	r_k (%)	$\dot{B}_{D,k}$ (mPts/h)	$\dot{Y}_k$ (mPts/h)	$f_{b,k}$ (%)	$r_{b,k}$ (%)
AC	43.91	41.84	2.076	95	4.72	126.8	975.7	88.5	43.2	45676	360.9	0.78	5
CC	117.9	90.39	27.52	77	23.34	1180	4.524	0.38	30.6	405172	964.7	0.23	71
GT	72.92	68.91	4.004	95	5.5	277.8	126.4	31.3	8.5				
HRSG	16.52	14.9	1.62	91	9.8	158.2	216.1	54.6	26	38424	260.4	0.614	10.95
BP ST	0.36	0.3588	0.021	94	5.9	8.427	119	93	3	1596	1133	41	19.45
Cond ST	42.36	36.96	3.2	87	12.7	696	507	42	42.2	147036	2643	1.7	15.2

Table 10 Single-pressure reheat arrangement using 500 mirrors

Device	$\dot{E}_{F,k}$ (MW)	$\dot{E}_{P,k}$ (MW)	$\dot{E}_D$ (MW)	ε_k (%)	$y_{D,k}$ (%)	$\dot{C}_{D,k}$ ($/h)	$\dot{Z}_k$ ($/h)	f_k (%)	r_k (%)	$\dot{B}_{D,k}$ (mPts/h)	$\dot{Y}_k$ (mPts/h)	$f_{b,k}$ (%)	$r_{b,k}$ (%)
AC	43.91	41.84	2.076	95	4.73	140.5	1212	89.6	47.7	45676	360.9	0.78	75
CC	117.9	90.39	27.52	77	23.34	1303	5.62	0.42	30.5	405172	964.7	0.23	71.21
GT	72.92	68.91	4.004	95	5.5	306.9	157.1	33.8	8.7				
Solar	3.89	2.084	1.78	54	45.16	498.8	972	66	253	186373	57890	23	112
HRSG	17.72	14.97	2.75	84	15.53	267.6	152.8	34.5	28.2	54598	127.9	0.23	18.42
Cond ST	14.24	12.89	1.38	90	9.7	183.9	226.4	53.3	23	34313	866.5	2.5	11

Table 11 Dual-pressure reheat arrangement using 500 mirrors

Device	$\dot{E}_{F,k}$ (MW)	$\dot{E}_{P,k}$ (MW)	$\dot{E}_D$ (MW)	ε_k (%)	$y_{D,k}$ (%)	$\dot{C}_{D,k}$ ($/h)	$\dot{Z}_k$ ($/h)	f_k (%)	r_k (%)	$\dot{B}_{D,k}$ (mPts/h)	$\dot{Y}_k$ (mPts/h)	$f_{b,k}$ (%)	$r_{b,k}$ (%)
AC	43.91	41.84	2.076	95	4.73	129.1	1017	88.8	44	45676	360.9	0.78	5
CC	117.9	90.39	27.52	77	23.34	1201	4.715	0.4	30.6	405172	964.7	0.23	71.21
GT	72.92	68.91	4.004	95	5.5	282.5	131.8	31.8	8.5				
Solar	3.87	2.084	1.786	54	46.16	459	717.98	63.9	237	186373	57890	23.7	112
HRSG	18.61	16.11	2.5	87	13.42	231	219	48.7	30.2	58964	570.1	0.95	15.66
Back pressure ST	1.986	1.873	0.113	94	5.7	14.82	137.3	90.3	62.1	3300	1177	26.28	8.2
Cond ST	13.38	12.08	1.3	90	9.7	167.8	318.9	65.5	31.2	37418	1432	3.6	11.15

Table 12 Triple-pressure reheat arrangement using 500 mirrors

Device	$\dot{E}_{F,k}$ (MW)	$\dot{E}_{P,k}$ (MW)	$\dot{E}_D$ (MW)	ε_k (%)	$y_{D,k}$ (%)	$\dot{C}_{D,k}$ ($/h)	$\dot{Z}_k$ ($/h)	f_k (%)	r_k (%)	$\dot{B}_{D,k}$ (mPts/h)	$\dot{Y}_k$ (mPts/h)	$f_{b,k}$ (%)	$r_{b,k}$ (%)
AC	43.91	41.84	2.076	95	4.72	125.7	956.9	88.4	42.7	45676	360.9	0.78	5
CC	117.9	90.39	27.52	77	23.34	1170	4.43	0.37	30.6	405172	964.7	0.23	71
GT	72.92	68.91	4.004	95	5.5	275.5	124	31	8.4				
Solar	3.78	2.084	1.786	54	46.16	447.8	767.85	63.2	232	186373	57860	23.7	112
HRSG	19.11	16.57	2.532	90	13.25	225	211.95	84.5	29.7	59764	260.4	0.43	15.34
Back pressure ST	0.133	0.1256	0.0074	94	5.6	2.83	120.3	97	258	595.5	1125	65	17.18
Cond ST	15.66	13.72	1.94	88	12.41	235	434.3	64.9	40.3	54910	2029	3.5	14

Table 13 Single-pressure reheat arrangement using 1000 mirrors

Device	$\dot{E}_{F,k}$ (MW)	$\dot{E}_{P,k}$ (MW)	$\dot{E}_D$ (MW)	ε_k (%)	$y_{D,k}$ (%)	$\dot{C}_{D,k}$ ($/h)	$\dot{Z}_k$ ($/h)	f_k (%)	r_k (%)	$\dot{B}_{D,k}$ (mPts/h)	$\dot{Y}_k$ (mPts/h)	$f_{b,k}$ (%)	$r_{b,k}$ (%)
AC	43.91	41.84	2.076	95	4.73	138.3	1174	89.5	47.1	45676	360.9	0.78	75
CC	117.9	90.39	27.52	77	23.34	1283	5.44	0.42	30.5	405172	964.7	0.23	71.21
GT	72.92	68.91	4.004	95	5.5	302.2	152.1	33.8	8.7				
Solar	7.687	4.662	3.025	61	39.36	418.7	1056	71.6	228	158907	115000	42	111
HRSG	20.64	17.43	3.206	84	15.53	307	166.1	35.1	28.3	75129	127	0.17	18.42
Cond ST	16.61	15	1.61	90	9.7	211	225	51.6	22.2	47090	938	1.9	11

Table 14 Dual-pressure reheat arrangement using 1000 mirrors

Device	$\dot{E}_{F,k}$ (MW)	$\dot{E}_{P,k}$ (MW)	$\dot{E}_D$ (MW)	ε_k (%)	$y_{D,k}$ (%)	$\dot{C}_{D,k}$ ($/h)	$\dot{Z}_k$ ($/h)	f_k (%)	r_k (%)	$\dot{B}_{D,k}$ (mPts/h)	$\dot{Y}_k$ (mPts/h)	$f_{b,k}$ (%)	$r_{b,k}$ (%)
AC	43.91	41.84	2.076	95	4.73	128	996	88.6	43.6	45676	360.9	0.78	5
CC	117.9	90.39	27.52	77	23.34	1191	4.62	0.4	30.6	405172	964.7	0.23	71.21
GT	72.92	68.91	4.004	95	5.5	280.4	129.2	31.5	8.5				
Solar	7.687	4.662	3.025	61	39.36	388.5	897	69.8	214	158907	115000	42	111
HRSG	21.36	18.19	3.164	85	14.82	269.3	215	44.4	31.3	74141	570.1	0.76	17.53
Back pressure ST	2.14	2.024	0.116	95	5.4	14.18	134.4	90.5	60	3438	1176	25.5	7.6
Cond ST	15.2	13.73	1.474	90	9.7	176	317.3	64.3	30.1	42812	1465	3.3	11.11

Table 15 Triple-pressure reheat arrangement using 1000 mirrors

Device	$\dot{E}_{F,k}$ (MW)	$\dot{E}_{P,k}$ (MW)	$\dot{E}_{D}$ (MW)	ε_k (%)	$y_{D,k}$ (%)	$\dot{C}_{D,k}$ ($/h)	$\dot{Z}_k$ ($/h)	f_k (%)	r_k (%)	$\dot{B}_{D,k}$ (mPts/h)	$\dot{Y}_k$ (mPts/h)	$f_{b,k}$ (%)	$r_{b,k}$ (%)
AC	**43.91**	**41.84**	**2.076**	**95**	**4.72**	**124.6**	**939**	**88.3**	**42.4**	**45676**	**360.9**	**0.78**	**5**
CC	117.9	90.39	27.52	77	23.34	1161	4.35	0.37	30.6	405172	964.7	0.23	71
GT	**72.92**	**68.91**	**4.004**	**95**	**5.5**	**273**	**121.7**	**30.8**	**8.4**				
Solar	7.678	4.662	3.025	61	39.36	379	844.8	69	209	158907	115000	42	111
HRSG	**21.76**	**18.28**	**3.5**	**84**	**16**	**284**	**207.32**	**42.3**	**33**	**81530**	**260.4**	**0.31**	**19.1**
Back pressure ST	0.137	0.1301	0.0073	95	5.6	2.81	118	97	242	645	1125	63	15.46
Cond ST	**17.23**	**15.14**	**2.092**	**88**	**12.14**	**238.6**	**430.6**	**64.4**	**38.8**	**60714**	**2062**	**3.3**	**14.3**

8. Conclusion

In this study, the heat recovery of Kashan Turbo-compressor station as a real case study has been considered through solar preheating of feed water and exergy recovery of hot gases of gas turbines. In this regard, a solar tower system, a heat recovery steam generator, and a steam turbine have been added. Three different configurations of HRSG have been investigated. To better evaluation of the proposed system, thermodynamic, exergetic, exergoeconomic, and exergoenvironmental analyses have been performed by the developed computer program. The results of the exergoenvironmental analysis show that the rate of exergy destruction for the environmental impact is higher for the combustion chamber than for other equipment integrated with the system. Because the combustion chamber has an irreversible chemical reaction, it significantly contributes to the exergy destruction of the combined system. As can be seen from the results, the investigation has been done for three pressure modes in the heat recovery generator and the solar mode. The results of the environmental analysis of the single-pressure section in the regenerator show that the combustion chamber has a more significant impact on the environment than other equipment, with a large share of exergy destruction. Also, the environmental factor for this equipment shows that the contribution of exergy destruction in this equipment is very high. In other modes, the environmental analysis of the system has been carried out, and the results show that with the addition of equipment to the system and working pressures in the heat recovery generator, the environmental effects of the components have improved. This work investigates the influence of the number of mirrors on exergy destruction, environmental impacts, and the cost of exergy destruction in a different configuration of HRSG. In addition, the comparison of an integrated system with and without solar energy has been evaluated with exergetic, exergoeconomic, and exergoenvironmental analyses. The results of the economic section for the integrated system show that considering the large share of exergy destruction for the combustion chamber, the economical parameters of this equipment are much higher than other equipment. For example, in Table 2, the cost rate for exergy destruction for the combustion chamber in the integrated system with the double-pressure recovery generator is equal to 1212 $/h. This rate is much higher than other equipment such as air compressors or gas turbines. Also, this value is higher than other equipment in the case of combining this system with a solar tower.

In future study, an advanced exergy analysis can be done based on simultaneous, endogenous/exogenous/available, and unavoidable parts. Furthermore, dynamic exergetic and exergoeconomic analyses can be performed.

Appendix A: Solar section

Table 16 Equations used in solar section. [28, 29]

$\mathrm{EOT} = 0.258\cos(x) - 7.416\sin(x) - 3.648\cos(2x) - 9.228\sin(2x)\ \ (\mathrm{min})$	$\alpha = \sin^{-1}(\sin(\delta)\sin(\phi) + \cos(\delta)\cos\omega\sin(f))$
$x = \frac{(360(N-1))}{365.242}$	$\theta_z = 90 - \alpha$
$t_s = LCT + \frac{EOT}{60} - LC$	$A' = \sin^{-1}(\frac{-\cos\delta\sin\omega}{\cos\alpha})$ If $\cos\omega^3 \frac{\tan\delta}{\cos\alpha}$ $A = 180 - A'$ else $A = 360 + A'$

$LC = \frac{A - B}{15}$ A = Local longitude B = Longitude of standard time zone meridian	$\eta_{cos} = 0.5\cos^{-1}\left(\frac{(Z_0 - Z_1)\sin\alpha - e_1\cos\alpha\sin A - n_1\cos\alpha\cos A}{\sqrt{(Z_0 - Z_1)^2 + {e_1}^2 + {n_1}^2}}\right)$
Longitude of standard time zone meridian $= 15 \times GMT$	If Dist<1000 $\eta_{atten} = 0.99321 - 0.0001176 \times dist - 1.97 \times 10^{-8} \times dist^2$ Else $\eta_{atten} = e^{(-0.0001106 \times dist)}$
$\omega = 15(t_s - 12)$	$\Delta R = HM(1.44 \times \cot(\theta_L) - 1.094 + 3.068.\theta_L - 1.1256.{\theta_L}^2)$
$\delta = \sin^{-1}(0.39795\cos(0.98563(N - 173)))$	$\Delta A = WM(1.749 + 0.6396 \times \theta_L + \frac{0.2873}{\theta_L - 0.04902}$
$h = \left\lvert\frac{1}{15}\cos^{-1}(-\tan(\text{Latitude}) \times \tan(23.44.\sin(360\frac{N + 284}{365})))\right\rvert$	$\theta_L = \tan^{-1}(\frac{1}{r})$ "rad"
Sunrise $=$ noon $-$ h Sunset $=$ noon $+$ h	

Appendix B

Purchased Equipment Cost

The component cost will vary due to the change in thermodynamic parameters. Therefore, we need to form functions according to the thermodynamic variables .Some of the components are formulated in Table 17, but for some others, because the sources were not mentioned, some reliable constant data were used [24].

Table 17 Purchased equipment cost in $

Component	Reference	PEC
Compressor	[19]	$PEC_{AC} = \left(\frac{C_{11}\dot{m}_{air}}{C_{12} - \eta_{sc}}\right)\left(\frac{p_{2g}}{p_{1g}}\right)\ln\left(\frac{p_{2g}}{p_{1g}}\right)$
Combustion Chamber	[19]	$PEC_{CC} = \left(\frac{C_{21}\dot{m}_{air}}{C_{22} - \frac{p_{3g}}{p_{2g}}}\right)[1 + \exp(C_{23}T_{3g} - C_{24})]$
Gas Turbine	[19]	$PEC_{GT} = \left(\frac{C_{31}\dot{m}_g}{C_{32} - \eta_{st}}\right)\ln\left(\frac{p_{3g}}{p_{4gGT}}\right)[1 + \exp(C_{33}T_{3g} - C_{34})]$
Single pressure HRSG	[27]	$PEC_{HRSG} = C_{51}\left[\left(\frac{\dot{Q}_{ec}}{\Delta T_{lm,ec}}\right)^{0.8} + \left(\frac{\dot{Q}_{ev}}{\Delta T_{lm,ev}}\right)^{0.8}\right] + C_{52}\dot{m}_{st} + C_{53}\dot{m}_g^{1.2}$
Dual pressure HRSG	[27]	$PEC_{HRSG_{2p}} = (5.805 - 0.1653 \times 10 + 0.0153 \times m_g) \times 10^6$
Triple pressure HRSG	[27]	$PEC_{HRSG_{3p}} = (5.805 - 0.1653 \times 10 + 0.0153 \times m_g) \times 10^6$
Solar tower	[27]	$PEC_{tower} = (C_{61} \times \exp(C_{62} \times 150))$
Solar field	[27]	$PEC_{Heliostats} = C_{71} \times A_{mir}$
Receiver	[27]	$PEC_{receiver} = 3330000$ [$]
Back pressure steam turbine	[27]	$PEC_{BPST} = (6.191 - 0.005573 \times m_{ST_{in}} - 0.1156 \times P_{ST_{in}} - 3.743 \times 10^{-6} \times {m_{ST_{in}}}^2 + 0.0003415 \times m_{ST_{in}} \times P_{ST_{in}} + 0.005948 \times {P_{ST_{in}}}^2) \times 10^6$
Condensing steam turbine	[27]	$PEC_{LPST} = (3.165 + 0.1048 \times m_{ST_{in}} + 0.01636 \times P_{ST_{in}}) \times 10^6$
High pressure pump	[24]	$PEC_{HPP} = 200000$ [$]
Medium pressure pump	[24]	$PEC_{IPP} = 150000$[$]
Low pressure pump	[24]	$PEC_{LPP} = 50000$ [$]
Other equipment	[19]	$PEC_{Other} = 942000$ [$]

Some constants used in the equations in Table 17 are shown in Table 18.

Table 18 Values of coefficients used in Table 17

Compressor	$C_{11} = 71.10$ \$/(kg/s)	$C_{12} = 0.9$
Combustion Chamber	$C_{21} = 46.08$ \$/(kg/s)	$C_{22} = 0.995$
	$C_{23} = 0.018$ (K^{-1})	$C_{24} = 26.4$
Gas Turbine	$C_{31} = 479.34$ \$/(kg/s)	$C_{32} = 0.92$
	$C_{33} = 0.036$ (K^{-1})	$C_{34} = 54.4$
HRSG	$C_{51} = 6570$ \$/(kW/K)$^{0.8}$	
	$C_{52} = 21276$ \$/(kg/s)	
	$C_{53} = 1184.4$ \$/(kg/s)$^{1.2}$	
Tower	$C_{61} = 0.78232e6$ $C_{62} = 0.01130$	

The above equations, $\dot{m}_{air}$, $\dot{m}_g$ and $\dot{m}_{ST}$ indicate the mass flow rate of air, combustion products, and steam/water in each component respectively. η_{sc} and η_{st} show the isentropic efficiency of the compressor and turbine respectively. $\Delta T_{lm,ec}$ and $\Delta T_{lm,ev,SH}$ indicate the Logarithmic mean temperature difference in the economizer, evaporator, and superheater in the single pressure reheat boiler. $\Delta T_{lm,ec}$ and $\Delta T_{lm,ev,SH}$ indicate the Logarithmic mean temperature difference in the economizer, evaporator, and superheater in the single pressure reheat boiler. The governing equations in dual and triple-pressure reheat boilers are simpler. $\dot{Q}_{ec}$ and $\dot{Q}_{ev,SH}$ indicate the heat transfer rate in the economizer and evaporator and superheater respectively [19].

$$\dot{Q}_{ec} = \dot{m}_{ST}(h_{3s} - h_{2s})$$
$$\dot{Q}_{ev,SH} = \dot{m}_{ST}(h_{5s} - h_{3s})$$
$$\Delta T_{lm,ec} = \frac{(T_{g5} - T_{3s}) - (T_{g6} - T_{2s})}{\ln \frac{T_{g5} - T_{3s}}{T_{g6} - T_{2s}}}$$
$$\Delta T_{lm,ev,SH} = \frac{(T_{g4} - T_{5s}) - (T_{g5} - T_{3s})}{\ln \frac{T_{g4} - T_{5s}}{T_{g5} - T_{3s}}}$$

Appendix C:

The amount of $\dot{B}_{Fuel}$ fuel which is pure methane equals [31]:

$$\dot{B}_{Fuel} = 180 \times \dot{m}_{Fuel} \times 10^{-3} \times 3600 \qquad (\frac{Pts}{h})$$

Table 19 shows the environmental impact rate for each component.

Table 19 Environmental impact rate for each component

Component	$\dot{Y}_k$ (Pts of Eco-indicator 99) (Pts/h)	Reference	Independent variables
Compressor	$\dot{Y}_{AC} = (-0.0076 \times P_{net}^2 + 13.558 \times P_{net} - 18.583) \times \frac{130.88 \times CRF}{\tau}$	[27]	P_{net} gas turbine net power (MW)
Combustion chamber and gas turbine	$\dot{Y}_{CC+GT} = (-0.0051 \times P_{net}^2 + 3.582 \times P_{net} + 70.438) \times \frac{704 \times CRF}{\tau}$	[27]	P_{net} gas turbine net power (MW)
Solar receiver	$\dot{Y}_{solar} = \frac{14 \times \dot{Q}_{solar} \times 10^{-3}}{\tau_{solar} \times N}$	[27]	$\dot{Q}_{solar}$ Heat transferred to the combustion gases (KW)
Single pressure HRSG	$\dot{Y}_{HRSG-1p} = \begin{pmatrix} -13.37 - 1.893 \times \Delta T_{pinch} \\ +1.945 \times m_{exhuast} \end{pmatrix} \times \frac{104 \times CRF}{\tau}$	[27]	$m_{exhuast}$ combustion gases (kg/s) and pinch temperature (ΔT_{pinch})
Dual-pressure HRSG	$\dot{Y}_{HRSG-2p} = \begin{pmatrix} 715.5 - 27.88 \times \Delta T_{pinch} \\ +2.143 \times m_{exhuast} \end{pmatrix} \times \frac{104 \times CRF}{\tau}$	[27]	

Triple-pressure HRSG	$\dot{Y}_{HRSG-3p} = \begin{pmatrix} 146.8 - 5.857 \times \Delta T_{pinch} \\ +2.229 \times m_{exhuast} \end{pmatrix} \times \frac{104 \times CRF}{\tau}$	[27]	
Steam turbine back pressure	$\dot{Y}_{BPST} = \begin{pmatrix} 189.7 + 0.2677 \times \dot{m}_s \\ -3.675 \times P_{in} - 0.0002562 \times {\dot{m}_s}^2 + \\ 0.008919 \times \dot{m}_s \times P_{in} + 0.022 \times {P_{in}}^2 \end{pmatrix} \times \frac{704 \times CRF}{\tau}$	[27]	$\dot{m}_s$:steam flow rate(kg/s) P_{in}: input pressure(bar)
Steam turbine condensing	$\dot{Y}_{LPST} = (78.57 + 4.486 \times \dot{m}_s + 0.5066 \times P_{in}) \times \frac{704 \times CRF}{\tau}$	[27]	$\dot{m}_s$:steam flow rate (kg/s) P_{in}: input pressure (bar)

Nomenclature

LHV	Lower heating value
C_P	Specific heat at constant pressure
e	Specific exergy
h	Specific enthalpy
$\dot{m}$	Mass flow rate
P	Pressure
T	Temperature
$\dot{W}$	Power
Z	Cost associated with a component

Greek Letters

ε_{ap}	Air pre-heater effectiveness
η_{sc}	Compressor isentropic efficiency
η_{st}	Gas turbine isentropic efficiency
η_{hrsg}	HRSG first law efficiency

Subscripts

air	Stream of air
ap	Air preheater
sc	Compressor
st	Turbine
fuel	Fuel
gas	Stream of combustion gases
steam	Flow of feed water/steam
total	Total plant

References

Khoshgoftar Manesh, M.H., et al., *Exergoeconomic Evaluation of Desalinated Water Production in Pipeline Gas Station*, in *Proceedings of the 3rd Gas Processing Symposium*, A. Aroussi and F. Benyahia, Editors. 2012, Elsevier: Oxford. p. 191-198.

Shahzad, M.W., et al., *A multi evaporator desalination system operated with thermocline energy for future sustainability.* Desalination, 2018. **435**: p. 268-277.

Askari, I.B. and M. Ameri, *Solar Rankine Cycle (SRC) powered by Linear Fresnel solar field and integrated with Multi Effect Desalination (MED) system.* Renewable Energy, 2018. **117**: p. 52-70.

Elsayed, M.L., et al., *Transient performance of MED processes with different feed configurations.* Desalination, 2018. **438**: p. 37-53.

Wu, L., Y. Hu, and C. Gao, *Optimum design of cogeneration for power and desalination to satisfy the demand of water and power.* Desalination, 2013. **324**: p. 111-117.

Shahzad, M.W., et al., *Multi effect desalination and adsorption desalination (MEDAD): A hybrid desalination method.* Applied Thermal Engineering, 2014. **72**(2): p. 289-297.

o, *Multi-objective optimization of MED-TVC-RO hybrid desalination system based on the irreversibility concept.* Desalination, 2017. **402**: p. 97-108.

Askari, I.B. and M. Ameri, *Techno economic feasibility analysis of Linear Fresnel solar field as thermal source of the MED/TVC desalination system.* Desalination, 2016. **394**: p. 1-17.

Dastgerdi, H.R., P.B. Whittaker, and H.T. Chua, *New MED based desalination process for low grade waste heat.* Desalination, 2016. **395**: p. 57-71.

Mokhtari, H., M. Sepahvand, and A. fasihfar, *Thermoeconomic and exergy analysis in using hybrid systems (GT+MED+RO) for desalination of brackish water in Persian Gulf.* Desalination, 2016. **399**: p. 1-15.

Kostowski, W.J., et al., *Energy and exergy recovery in a natural gas compressor station – A technical and economic analysis.* Energy Conversion and Management, 2015. **104**: p. 17-31.

Bianchi, M., et al., *Techno-Economic Analysis of ORC in Gas Compression Stations Taking Into Account Actual Operating Conditions.* Energy Procedia, 2017. **129**: p. 543-550.

Gómez-Aláez, S.L., et al., *Off-design study of a waste heat recovery ORC module in gas*

pipelines recompression station. Energy Procedia, 2017. **129**: p. 567-574.

Yanvarev, I.A., A.D. Vanyashov, and A.V. Krupnikov, *Improving Gas Cooling Technology at its Compression in the Booster Compressor Station*. Procedia Engineering, 2016. **152**: p. 233-239.

Akbari, A.D. and S.M.S. Mahmoudi, *Thermoeconomic performance and optimization of a novel cogeneration system using carbon dioxide as working fluid*. Energy Conversion and Management, 2017. **145**: p. 265-277.

Hanafi, A.S., et al., *Thermo-Economic Analysis of Combined Cycle MED-TVC Desalination System*. Energy Procedia, 2015. **75**: p. 1005-1020.

Dabwan, Y.N. and E.M.A. Mokheimer, *Optimal integration of linear Fresnel reflector with gas turbine cogeneration power plant*. Energy Conversion and Management, 2017. **148**: p. 830-843.

Rezaei, A., et al., *Economic evaluation of Qeshm island MED-desalination plant coupling with different energy sources including fossils and nuclear power plants*. Desalination, 2017. **422**: p. 101-112.

Bejan, A., G. Tsatsaronis, and M. Moran, *Thermal design and optimization*. Vol. 1. 1996.

Soltani, R., et al., *Multi-objective optimization of a solar-hybrid cogeneration cycle: Application to CGAM problem*. Energy Conversion and Management, 2014. **81**: p. 60-71.

Bassily, A.M., *Modeling, numerical optimization, and irreversibility reduction of a dual-pressure reheat combined-cycle*. Applied Energy, 2005. **81**(2): p. 127-151.

Bassily, A.M., *Modeling, numerical optimization, and irreversibility reduction of a triple-pressure reheat combined cycle*. Energy, 2007. **32**(5): p. 778-794.

Kotas, T.J., *Chapter 2 - Basic exergy concepts*, in *The Exergy Method of Thermal Plant Analysis*, T.J. Kotas, Editor. 1985, Butterworth-Heinemann. p. 29-56.

Colpan, C., *Exergy analysis of combined cycle cogeneration systems*. Middle East Technical University, 2005.

Çolpan, C.Ö., *Exergy analysis of combined cycle cogeneration systems*. 2005, Middle east technical university.

26. Bejan, A., G. Tsatsaronis, and M. Moran, *Thermal Design and Optimization John Wiley and Sons*. Inc. New York, 1996.

Tsatsaronis, G. and T. Morosuk, *A General Exergy-Based Method for Combining a Cost Analysis With an Environmental Impact Analysis: Part II — Application to a Cogeneration System*. 2008(48692): p. 463-469.

Segal, A. and M. Epstein, *The optics of the solar tower reflector*. Solar Energy, 2001. **69**: p. 229-241.

Yogev, A., et al., *Solar "tower reflector" systems: a new approach for high-temperature solar plants*. International journal of hydrogen energy, 1998. **23**(4): p. 239-245.

Khoshgoftar Manesh, M.H. and M. Ameryan, *Optimal design of a solar-hybrid cogeneration cycle using Cuckoo Search algorithm*. Applied Thermal Engineering, 2016. **102**: p. 1300-1313.

Petrakopoulou, F., et al., *Exergoeconomic and exergoenvironmental analyses of a combined cycle power plant with chemical looping technology*. International Journal of Greenhouse Gas Control, 2011. **5**(3): p. 475-482.